Research Article | Vol. 6, No. 9 | 1 Sep 2016 | OPTICAL MATERIALS EXPRESS 2769

Optical Materials EXPRESS

Efficient near-infrared downconversion and energy transfer mechanism in Tb^{4+}-Yb^{3+} co-doped $NaYF_4$ nanoparticles

Biao Zheng,[1] Lin Lin,[1,2,3,4] Senyuan Xu,[1] Zhezhe Wang,[1,2,3] Zhuohong Feng,[1,2,3] and Zhiqiang Zheng[1,2,3,*]

[1]*College of Physics and Energy, Fujian Normal University, Fuzhou 350117, China*
[2]*Fujian Provincial Key Laboratory of Quantum Manipulation and New Energy Materials, Fuzhou 350117, China*
[3]*Fujian Provincial Collaborative Innovation Center for Optoelectronic Semiconductors and Efficient Devices, Xiamen 361005, China*
[4]*llin@fjnu.edu.cn*
**zqzheng@fjnu.edu.cn*

Abstract: Tb^{4+}-Yb^{3+} co-doped $NaYF_4$ nanoparticles (NPs) are prepared by sintering the as-synthesized $NaYF_4$:Tb^{3+}, Yb^{3+} NPs at 380°C under air atmosphere. The oxidization of Tb^{3+} ions to Tb^{4+} ions in $NaYF_4$ NPs after sintering is demonstrated through X-ray photoelectron spectroscopy (XPS). The near-infrared (NIR) downconversion (DC) luminescence of Tb^{4+}-Yb^{3+} couple is measured and investigated for the first time. The results show that DC luminescence of Tb^{4+}-Yb^{3+} couple enhance obviously compared with Tb^{3+}-Yb^{3+} couple in as-synthesized sample. The enhancement factor is about 14 and 19 excited at 379nm and 487nm, respectively. On analyzing the exponential dependence of NIR fluorescence intensity on the pumping power, we reveal that the energy transfer (ET) mechanism from Tb^{4+} to Yb^{3+} in $NaYF_4$ NPs occurs by the single-step ET process. Our study may provide a promising DC layer on the top of silicon-based solar cells to improve the photovoltaic conversion efficiency.

OCIS codes: (160.5690) Rare-earth-doped materials; (250.5230) Photoluminescence; (260.2160) Energy transfer; (160.4236) Nanomaterials.

References and links

1. L. Aarts, B. Van der Ende, and A. Meijerink, "Downconversion for solar cells in $NaYF_4$: Er, Yb," J. Appl. Phys. **106**(2), 023522 (2009).
2. D. Chen, Y. Yu, Y. Wang, P. Huang, and F. Weng, "Cooperative energy transfer up-conversion and quantum cutting down-conversion in Yb^{3+}: TbF_3 nanocrystals embedded glass ceramics," J. Phys. Chem. C **113**(16), 6406–6410 (2009).
3. L. Lin, J. Chen, C. Deng, L. Tang, D. Chen, and L. Cao, "Broadband near-infrared quantum-cutting by cooperative energy transfer in Yb^{3+}-Bi^{3+} co-doped $CaTiO_3$ for solar cells," J. Alloys Compd. **640**, 280–284 (2015).
4. X. Chen, S. Li, G. J. Salamo, Y. Li, L. He, G. Yang, Y. Gao, and Q. Liu, "Sensitized intense near-infrared downconversion quantum cutting three-photon luminescence phenomena of the Tm^{3+}:ion activator in Tm^{3+}:Bi^{3+}:$YNbO_4$ powder phosphor," Opt. Express **23**(3), A51–A61 (2015).
5. L. Lin, H. Lin, Z. Wang, J. Chen, R. Huang, X. Rao, Z. Feng, and Z. Zheng, "Quantum-cutting of KYF_4:Tb^{3+},Yb^{3+} under multiple excitations with high Tb^{3+} concentration," Opt. Mater. **36**(6), 1065–1069 (2014).
6. K. Deng, T. Gong, L. Hu, X. Wei, Y. Chen, and M. Yin, "Efficient near-infrared quantum cutting in $NaYF_4$: Ho^{3+}, Yb^{3+} for solar photovoltaics," Opt. Express **19**(3), 1749–1754 (2011).
7. B. Zheng, S. Xu, L. Lin, Z. Wang, Z. Feng, and Z. Zheng, "Plasmon enhanced near-infrared quantum cutting of KYF_4: Tb^{3+}, Yb^{3+} doped with Ag nanoparticles," Opt. Lett. **40**(11), 2630–2633 (2015).
8. Y. S. Xu, F. Huang, B. Fan, C. G. Lin, S. X. Dai, L. Y. Chen, Q. H. Nie, H. L. Ma, and X. H. Zhang, "Quantum cutting in Pr^{3+}-Yb^{3+} codoped chalcohalide glasses for high-efficiency c-Si solar cells," Opt. Lett. **39**(8), 2225–2228 (2014).
9. A. Guille, A. Pereira, C. Martinet, and B. Moine, "Quantum cutting in $CaYAlO_4$: Pr^{3+}, Yb^{3+}," Opt. Lett. **37**(12), 2280–2282 (2012).
10. I. Terra, L. Borrero-González, J. Carvalho, M. Terrile, M. Felinto, H. Brito, and L. Nunes, "Spectroscopic properties and quantum cutting in Tb^{3+}–Yb^{3+} co-doped ZrO_2 nanocrystals," J. Appl. Phys. **113**(7), 073105 (2013).

#269540 http://dx.doi.org/10.1364/OME.6.002769
Journal © 2016 Received 29 Jun 2016; revised 1 Aug 2016; accepted 1 Aug 2016; published 8 Aug 2016

Optical Materials EXPRESS

11. Z. Liu, N. Dai, L. Yang, and J. Li, "High-efficient near-infrared quantum cutting based on broadband absorption in Eu^{2+}–Yb^{3+} co-doped glass for photovoltaic applications," Appl. Phys. Adv. Mater. **119**(2), 553–557 (2015).
12. Y. Ying and Y. Ru-Dong, "Synthesis and characterization of tetravalent terbium complexes of alkali terbium hexaoxidoiodates," Polyhedron **11**(8), 963–966 (1992).
13. H. Ebendorff-Heidepriem and D. Ehrt, "Effect of Tb^{3+} ions on X-ray-induced defect formation in phosphate containing glasses," Opt. Mater. **18**(4), 419–430 (2002).
14. R. K. Verma, K. Kumar, and S. B. Rai, "Inter-conversion of Tb^{3+} and Tb^{4+} states and its fluorescence properties in MO–Al_2O_3: Tb (M = Mg, Ca, Sr, Ba) phosphor materials," Solid State Sci. **12**(7), 1146–1151 (2010).
15. Y. Liu, Y. Xia, Y. Jiang, M. Zhang, and X. Zhao, "Coupling effects of Au-decorated core-shell β-$NaYF_4$: Er/Yb@ SiO_2 microprisms in dye-sensitized solar cells: plasmon resonance versus upconversion," Electrochim. Acta **180**, 394–400 (2015).
16. Z. Li and Y. Zhang, "An efficient and user-friendly method for the synthesis of hexagonal-phase $NaYF_{(4)}$:Yb, Er/Tm nanocrystals with controllable shape and upconversion fluorescence," Nanotechnology **19**(34), 345606 (2008).
17. B. Chen, D. Peng, X. Chen, X. Qiao, X. Fan, and F. Wang, "Establishing the Structural Integrity of Core-Shell Nanoparticles against Elemental Migration using Luminescent Lanthanide Probes," Angew. Chem. Int. Ed. Engl. **54**(43), 12788–12790 (2015).
18. J. F. Moulder and R. C. King, *Handbook of X-ray Photoelectron Spectroscopy: A Reference Book of Standard Spectra for Identification and Interpretation of XPS Data* (Physical Electronics, 1995).
19. L. Lin, H. Lin, Z. Wang, B. Zheng, J. Chen, S. Xu, Z. Feng, and Z. Zheng, "Luminescence properties of alkali metal ions sensitized CaFCl: Tb^{3+} nanophosphors," J. Rare Earths **33**(10), 1026–1030 (2015).
20. J. Li, L. Chen, Z. Hao, X. Zhang, L. Zhang, Y. Luo, and J. Zhang, "Efficient Near-Infrared Downconversion and Energy Transfer Mechanism Of Ce^{3+}/Yb^{3+} Codoped Calcium Scandate Phosphor," Inorg. Chem. **54**(10), 4806–4810 (2015).
21. D. Yu, F. Rabouw, W. Boon, T. Kieboom, S. Ye, Q. Zhang, and A. Meijerink, "Insights into the energy transfer mechanism in Ce^{3+}– Yb^{3+} codoped YAG phosphors," Phys. Rev. B **90**(16), 165126 (2014).
22. Y.-S. Xu, F. Huang, B. Fan, C.-G. Lin, S.-X. Dai, L.-Y. Chen, Q.-H. Nie, H.-L. Ma, and X.-H. Zhang, "Quantum cutting in Pr^{3+}-Yb^{3+} codoped chalcohalide glasses for high-efficiency c-Si solar cells," Opt. Lett. **39**(8), 2225–2228 (2014).
23. J. Zhou, Y. Teng, X. Liu, S. Ye, X. Xu, Z. Ma, and J. Qiu, "Intense infrared emission of Er^{3+} in $Ca_8Mg(SiO_4)_4Cl_2$ phosphor from energy transfer of Eu^{2+} by broadband down-conversion," Opt. Express **18**(21), 21663–21668 (2010).

1. Introduction

The increasing demand for solar energy, due to its green and inexhaustible advantage, has put how to improve the photovoltaic conversion efficiency of solar cells at the forefront of research [1]. The mismatch between the solar spectrum and the band gap energy of silicon semiconductor limits the photovoltaic conversion efficiency of silicon-based solar cells, because photons with energy lower than the band gap cannot be absorbed, while for photons with energy larger than the band gap, the excess energy is lost by thermalization of hot charge carriers [2–4]. Herein, there are many routes to improve the conversion efficiency, and one of them is the downconversion (DC) [5–10]. The DC process can convert ultraviolet-visible (UV-Vis) photon (300-600nm) into near-infrared (NIR) photon (~1000nm), which can be efficiently absorbed by silicon-based solar cells [1].

RE^{3+}-Yb^{3+} (RE = Tb, Ho, and Pr) couple have been demonstrated with optical spectroscopy for NIR DC in various hosts [2, 6, 9]. However, these DC materials are still far from practical application, because the absorption of the sensitizer RE^{3+} ion arisen from the parity-forbidden $4f$-$4f$ transitions are naturally weak in intensity, narrow in bandwidth, and usually give emission in UV-Vis region [11]. In this article, we report an efficient NIR DC luminescence between Tb^{4+}-Yb^{3+} couple, which is observed for the first time to our knowledge. Tb^{4+} ion might be an ideal broadband sensitizer for Yb^{3+} ion due to its charge transfer (CT) state located at 300nm-600nm [12, 13]. This broad CT state covers the high-energy part of the solar spectrum and matches twice the energy of Yb^{3+} ion. Moreover, the Tb^{4+} ion has the same electron configuration as Gd^{3+} ion ($4f^7$). Thus, its excited $4f$ levels lie above the CT state, which result in that it absorbs high-energy photon but doesn't give any emission in UV-Vis region in any host materials [14]. Therefore, the sensitizer Tb^{4+} ion could efficiently transfer the absorbed energy to activator Yb^{3+} ion without any emission in UV-Vis

Optical Materials EXPRESS

region, which will provide a better NIR DC system for silicon-based solar cells to improve the photovoltaic conversion efficiency.

2. Experimental

We chose the inorganic fluoride hexagonal $NaYF_4$ nanoparticles (NPs) as DC host due to its low phonon frequencies and high chemical stability [15]. Hexagonal $NaYF_4$:15%Tb^{3+}, 10%Yb^{3+} NPs were synthesized through coprecipitation method as follows [16]: 0.4550g $YCl_3 \cdot 6H_2O$ (99.99%), 0.0776g $YbCl_3 \cdot 6H_2O$ (99.99%) and 0.1120g $TbCl_3 \cdot 6H_2O$ (99.99%) were mixed with 12ml oleic acid (OA, 90%) and 30ml 1-octadecene (ODE, 90%) in a 100ml flask and heated to 130°C to form a homogeneous solution, and then cooled down to room temperature. 20ml methanol (A.R.) solution containing 0.2g NaOH (A.R.) and 0.2963g NH_4F (A.R.) was slowly added into the flask and the mixture were stirred for 30min to ensure that all fluoride has consumed completely. Subsequently, the mixture was slowly heated to 130°C to evaporate methanol, then heated up to 300°C rapidly and maintained for 1h under argon atmosphere. After the solution was cooled down naturally, $NaYF_4$ NPs were precipitated from the solution with ethanol, washed with ethanol for three times, collected by centrifugation and baked in 60°C. Finally, the as-synthesized $NaYF_4$ NPs were sintered at 380°C under air atmosphere, yielding the final Tb^{4+}-Yb^{3+} co-doped $NaYF_4$ NPs. Sintering at 380°C could oxidize the Tb^{3+} ion to Tb^{4+} ion, and avoid the $NaYF_4$ lattice structure be destroyed [17]. The chemical reagents ($YCl_3 \cdot 6H_2O$, $YbCl_3 \cdot 6H_2O$, $TbCl_3 \cdot 6H_2O$, OA, and ODE) were purchased from Sigma-Adrich. Methanol, NaOH and NH_4F were supplied by Sinopharm Chemical Reagent Company (Shanghai). All chemicals were used directly without further purification.

As-prepared samples were characterized by X-ray diffraction (XRD, MiniFlexII, Rigaku), X-ray photoelectron spectroscopy (XPS, ESCALAB 250, Thermo Scientific), fluorescence spectra (Fluorolog 3-22 spectrofluorometer, Horiba Jobin Yvon), scanning electron microscope (SEM, SU8010, Hitachi). Specifically, the fluorescence spectra in the same figure were measured by the same spectrofluorometer in one experiment, with the same measuring conditions (temperature, slit width, placement of samples, optical path, etc). Thus, the intensity of these spectra in one figure is comparable.

3. Results and discussion

Figure 1(a) illustrates the XRD patterns of the $NaYF_4$: x%Tb,10%Yb (x = 5,10,15,20,30) NPs after sintering at 380°C for 2h. All of the experimental diffraction peaks match well with those of hexagonal $NaYF_4$ phase (JCPDS 16-0334), which indicates that the $NaYF_4$ lattice structure are not destroyed after 380°C sintering. In order to confirm that Tb^{3+} ions are oxidized to Tb^{4+} ions after sintering, the Tb 4d XPS spectrum of $NaYF_4$:15%Tb,10%Yb NPs after sintering is measured. As shown in Fig. 1(b), the photoelectron line at ~147 eV belongs to Tb^{3+} ions while the photoelectron line at ~150 eV belongs to Tb^{4+} ions [14, 18], which indicates part of Tb^{3+} ions are oxidized to Tb^{4+} ions during the sintering process. In addition, according to the inset of Fig. 1(b), the $NaYF_4$ NPs have an average diameter of ~20nm and a large specific surface, which will promote the oxidation of Tb^{3+} ions to Tb^{4+} ions. To distinguish from as-synthesized $NaYF_4$:Tb^{3+},Yb^{3+} NPs, we use $NaYF_4$:Tb^{4+},Yb^{3+} NPs to represent the $NaYF_4$ NPs after 380°C sintering.

Optical Materials EXPRESS

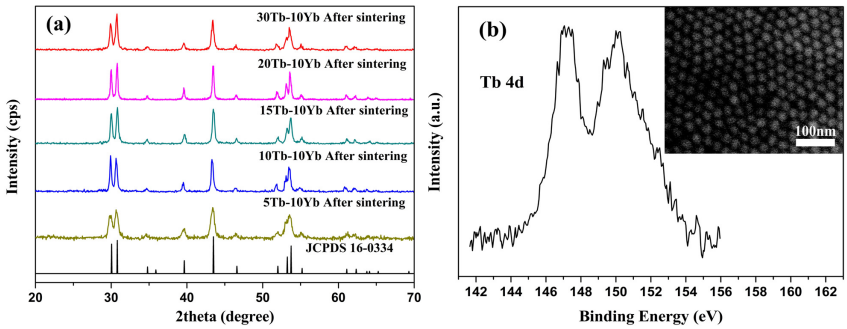

Fig. 1. (a) XRD patterns of the $NaYF_4$: *x*%Tb,10%Yb (*x* = 5,10,15,20,30) NPs after sintering. (b) Tb 4d photoelectron spectrum of $NaYF_4$:15%Tb,10%Yb NPs after sintering. Inset: SEM image of $NaYF_4$:15%Tb,10%Yb NPs before sintering.

Figure 2 shows the visible emission spectra (λ_{ex} = 379nm) and corresponding excitation spectra (λ_{em} = 544nm) of $NaYF_4$:Tb^{3+},Yb^{3+} NPs and $NaYF_4$:Tb^{4+},Yb^{3+} NPs. We can observe the intensity of major excitation peaks at 350, 368, 379, and 487nm (Tb^{3+}:$^7F_6 \rightarrow {}^5D_2$, $^5L_{10}$, $^5D_3$, $^5D_4$) and the major emission peaks at 490, 544, 585 and 620nm (Tb^{3+}:$^5D_4 \rightarrow {}^7F_j$ (j = 6, 5, 4, 3)) in $NaYF_4$:Tb^{4+},Yb^{3+} NPs decrease dramatically [7], which further indicates part of Tb^{3+} ions are oxidized to Tb^{4+} ions after sintering at 380°C. In addition, the excitation/emission peaks of Tb^{4+} ions aren't observed in $NaYF_4$:Tb^{4+},Yb^{3+} NPs, which is in agreement with that Tb^{4+} ion absorbs high-energy photon but doesn't give any emission in UV-Vis region [14].

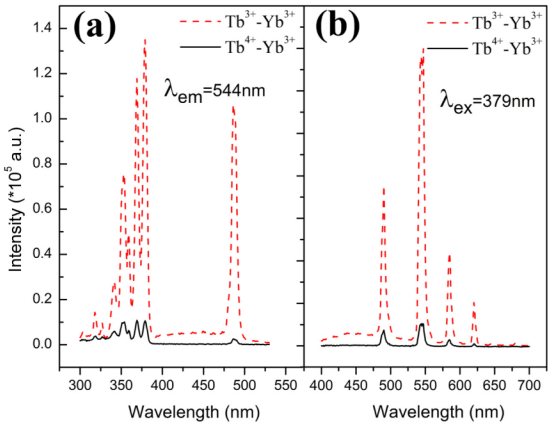

Fig. 2. (a) UV-Vis excitation spectra (λ_{em} = 544nm) and (b) emission spectra (λ_{ex} = 379nm) of $NaYF_4$: Tb^{3+}, Yb^{3+} NPs (dash lines) and $NaYF_4$: Tb^{4+}, Yb^{3+} NPs (solid lines).

In order to research the influence of Tb^{4+} ion on the NIR DC luminescence in $NaYF_4$ NPs, the NIR emission spectra of $NaYF_4$:Tb^{3+},Yb^{3+} NPs and $NaYF_4$:Tb^{4+},Yb^{3+} NPs under 379nm and 487nm excitation are measured. As shown in Fig. 3(a) and Fig. 3(b), it can be clearly observed that the major emission peak is located at 977nm, attributed to the $^2F_{5/2} \rightarrow {}^2F_{7/2}$ transitions of Yb^{3+} ion. Contrast with $NaYF_4$:Tb^{3+},Yb^{3+} NPs, the NIR emission intensity of Yb^{3+} ion in $NaYF_4$:Tb^{4+},Yb^{3+} NPs enhances obviously. The enhancement factor is about 14 and 19 excited at 379nm and 487nm, respectively.

Figure 3(c) illustrates the excitation spectra of $NaYF_4$:Tb^{3+},Yb^{3+} NPs and $NaYF_4$:Tb^{4+},Yb^{3+} NPs monitored at 977nm. Compared with the $NaYF_4$:Tb^{3+},Yb^{3+} NPs, the weak excitation peaks of Tb^{3+} ion still can be observed in the excitation spectrum of $NaYF_4$:Tb^{4+},Yb^{3+} NPs, indicating part of Tb^{3+} ions remains after sintering at 380°C. Moreover, a strong broad excitation band from 300nm to 600nm can be observed in the excitation spectrum of $NaYF_4$:Tb^{4+},Yb^{3+} NPs, which may arise from (i) Tb^{4+} ions; (ii) Tb^{3+}

Optical Materials EXPRESS

ions; (iii) oxygen defects; (iv) Yb^{2+} ions; (v) Yb^{3+} ions. Firstly, the possibility arising from Tb^{3+} ions can be easily excluded because Tb^{3+} ions doesn't have characteristic excitation band located at 300nm to 600nm. Secondly, if this broad excitation band is originated from oxygen defects, the oxygen defects will transfer absorbed energy to Tb^{3+} ions and we should observe an excitation band from 300nm to 600nm in the excitation spectrum of $NaYF_4$:Tb^{4+},Yb^{3+} NPs monitored the emission of Tb^{3+} ions at 544nm, which is opposite to the experimental result (See Fig. 2). Thus, the possibility arising from oxygen defects also can be excluded. To further confirm this broad excitation band is originated from Tb^{4+} ions, the excitation spectra monitored at 977nm of $NaYF_4$:Tb^{4+},Yb^{3+} NPs doped different Tb concentration are measured. As shown in Fig. 4(a), the excitation band isn't observed when only doped Yb^{3+} ions, which can exclude the possibility arising from Yb^{2+} ions or Yb^{3+} ions. Moreover, the excitation band intensity of $NaYF_4$:Tb^{4+},Yb^{3+} NPs increases with increasing doped Tb concentration from 0% to 15%, and then decreases with the further increase of doped Tb concentration mainly ascribed to the concentration quenching effect that Tb^{4+} ions migrate the absorbed energy to defects, which convincingly demonstrates that this broad excitation band stems from the CT transition of Tb^{4+} ions. In addition, from the inset of Fig. 4(a), the relative rate of Tb^{4+} and Tb^{3+} doesn't change with Tb concentration, because the relative rate of excitation peak area of the Tb^{4+} and Tb^{3+} is nearly unchanged doped with different Tb concentration. Therefore, we can conclude that an energy transfer (ET) from Tb^{4+} ion to Yb^{3+} ion occurs in $NaYF_4$ NPs after sintering.

In addition, the influence of sintering time on NIR DC luminescence in $NaYF_4$ NPs is investigated. As shown in Fig. 4(b), the NIR emission intensity of $NaYF_4$:Tb^{4+},Yb^{3+} NPs increases with increasing sintering time from 0h to 2h and then decreases with the further increase of sintering time. The increase NIR emission intensity is ascribed to that Tb^{3+} ions are oxidized to Tb^{4+} ions under sintering at air atmosphere, while the decrease intensity after further sintering is due to that oxygen defects will occur and absorb the energy [19].

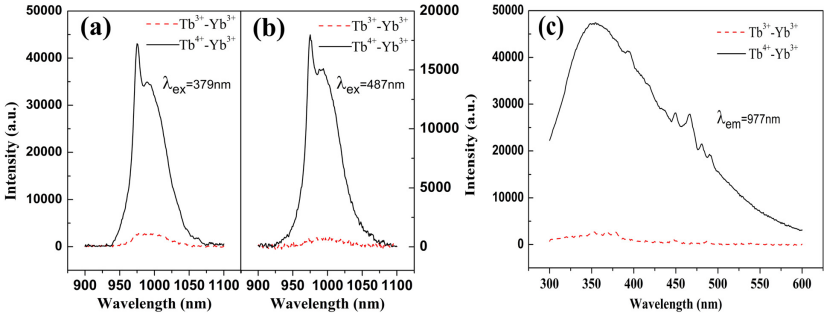

Fig. 3. (a),(b) NIR emission spectra under 379nm and 487nm excitation; (c) UV-Vis excitation spectra monitoring at 977nm of $NaYF_4$:Tb^{3+},Yb^{3+} NPs (dash lines) and $NaYF_4$:Tb^{4+}, Yb^{3+} NPs (solid lines), respectively.

Optical Materials EXPRESS

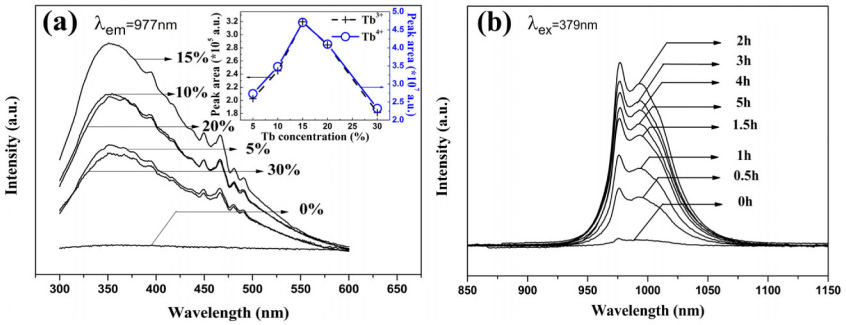

Fig. 4. (a) UV-Vis excitation spectra (λ_{em} = 977nm) of the $NaYF_4$:x%Tb^{4+},10%Yb^{3+} NPs. Inset: the excitation peak area of Tb^{3+} and Tb^{4+} in the $NaYF_4$: x%Tb^{4+}, 10%Yb^{3+} NPs (x = 0,5,10,15,20,30). (b) NIR emission spectra (λ_{ex} = 379nm) of $NaYF_4$:Tb^{4+},Yb^{3+} NPs under different sintering time.

Tb^{4+}-Yb^{3+} couple have a broad and strong excitation band in UV-Vis region, which may have two different ET mechanisms in the DC process, similar to Ce^{3+}-Yb^{3+} couple [20, 21]. One mechanism involves DC by cooperative ET, which would yield two NIR photons for each UV-Vis photon excitation. The other mechanism of single-step ET yields only a single NIR photon for each UV-Vis photon excitation. To judge the ET mechanism from Tb^{4+} ions to Yb^{3+} ions in $NaYF_4$ NPs, the pumping power dependence curves for the luminescence of Yb^{3+} ions at 977nm are measured and plotted on a double logarithmic scale. We know that the relationship between the NIR emission intensity (I) and pumping power (P) is $I \propto P^n$, where n is the corresponding photon number involved in the DC process [22, 23]. As shown in Fig. 5(a), the intensities of NIR emission exhibited linear dependence on the pumping power. The number of photon n determined from the slope coefficient of the linear-fitting line is 1.025 and 1.026 excited at 379nm and 487nm, respectively, which demonstrates the single-step ET mechanism in $NaYF_4$:Tb^{4+},Yb^{3+} NPs. In order to illustrate the NIR DC luminescence process of Tb^{4+}-Yb^{3+} couple in $NaYF_4$ NPs, the energy levels diagram of Tb^{4+} ion and Yb^{3+} ion are shown in Fig. 5(b). In this system, Tb^{4+} ion is doped as a sensitizer and Yb^{3+} ion is doped as an activator. Initially, the doped Tb^{4+} ions are excited at 379nm or 487nm from the ground level $^7F_6$ to the CT state. Then, the single-step ET process occurs from an excited Tb^{4+} ion to neighbor Yb^{3+} ion in the ground level. Finally, the NIR DC luminescence at 977nm is emitted from the transition $^2F_{5/2} \rightarrow {}^2F_{7/2}$ of the excited Yb^{3+} ion. It should be stressed that the CT transition of Tb^{4+} ion has a very broad and strong absorption but does not give any emission in UV-Vis region, which ensures that Tb^{4+} ion can efficiently transfer the absorbed high-energy to Yb^{3+} ion for NIR DC luminescence. Therefore, an efficient NIR DC luminescence is achieved through single-step ET process from Tb^{4+} ion to Yb^{3+} ion in $NaYF_4$ NPs.

Optical Materials EXPRESS

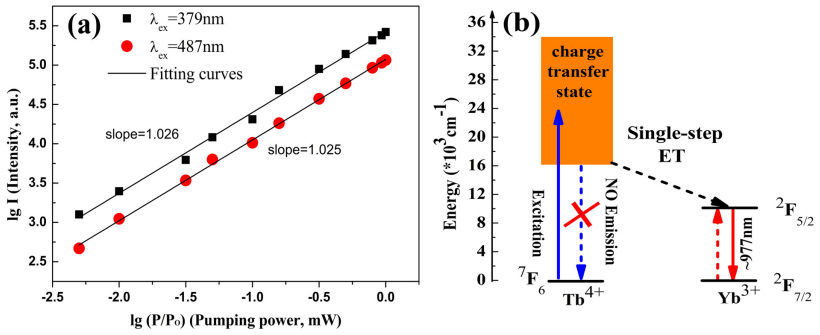

Fig. 5. (a) Log-log plot for dependency of 977nm NIR emission intensity on pumping power in $NaYF_4$:Tb^{4+},Yb^{3+} NPs excited at 379nm and 487nm, respectively. (b) Energy levels diagrams of Tb^{4+}-Yb^{3+} couple in the NIR DC energy transfer.

4. Conclusions

In summary, we use a facile strategy to prepare Tb^{4+}-Yb^{3+} co-doped $NaYF_4$ NPs by sintering the as-synthesized $NaYF_4$:Tb^{3+},Yb^{3+} NPs at 380°C under air atmosphere. Tb^{4+} ion appears attributed to the oxidation of Tb^{3+} ion during sintering process, which is demonstrated by XPS spectrum. The NIR DC luminescence of Tb^{4+}-Yb^{3+} couple is measured and investigated. The results show that the NIR DC luminescence of Tb^{4+}-Yb^{3+} couple has an efficient enhancement compared with Tb^{3+}-Yb^{3+} couple in as-synthesized sample. The enhancement factor is about 14 and 19 excited at 379nm and 487nm, respectively. This is due to that the broad and strong CT state of Tb^{4+} ion located at UV-Vis region absorbs high-energy photon but doesn't give any emission. We reveal that the ET mechanism from Tb^{4+} ions to Yb^{3+} ions in $NaYF_4$ NPs occurs by the single-step ET process through the exponential dependence curves of NIR fluorescence intensity on the pumping power. We also research the influence of sintering time on NIR DC luminescence and find the optimal sintering time is 2h. Our study may provide a promising DC layer for silicon-based solar cells to improve the photovoltaic conversion efficiency.

Funding

National Natural Science Foundation of China (NFSC) (11204039, 51202033); Natural Science Foundation of Fujian Province of China (2015J01243); Science Foundation of the Educational Department of Fujian Province of China (JA13084).